Check for updates

Contemporary decline in northern Indian Ocean primary production offset by rising atmospheric nitrogen deposition

Manon Malsang[1,2]*, Laure Resplandy[2,3]*, Laurent Bopp[4,5,6], Yangyang Zhao[3], Sam Ditkovsky[2], Fan Yang[3], Fabien Paulot[7] and Marina Lévy[1]*

[1]UMR7159 Laboratoire d'Océanographie et du Climat Expérimentals et Approches Numériques (LOCEAN), Institut Pierre-Simon Laplace (IPSL), Sorbonne Université, UB, Paris, France, [2]Department of Geosciences, Princeton University, Princeton, NJ, United States, [3]High Meadows Environmental Institute, Princeton University, Princeton, NJ, United States, [4]Laboratoire de Météorologie Dynamique, Sorbonne Université (CNRS), Paris, Île-de-France, France, [5]Laboratoire de Météorologie Dynamique, Institut Pierre-Simon Laplace, CNRS, École Normale Supérieure, Université PSL, Sorbonne Université, École Polytechnique, Paris, France, [6]Département de Géosciences, École Normale Supérieure, Paris, France, [7]Geophysical Fluid Dynamics Laboratory, National Oceanic and Atmospheric Administration, Princeton, NJ, United States

Since 1980, atmospheric pollutants in South Asia and India have dramatically increased in response to industrialization and agricultural development, enhancing the atmospheric deposition of anthropogenic nitrogen in the northern Indian Ocean and potentially promoting primary productivity. Concurrently, ocean warming has increased stratification and limited the supply of nutrients supporting primary productivity. Here, we examine the biogeochemical consequences of increasing anthropogenic atmospheric nitrogen deposition and contrast them with the counteracting effect of warming, using a regional ocean biogeochemical model of the northern Indian Ocean forced with atmospheric nitrogen deposition derived from an Earth System Model. Our results suggest that the 60% recent increase in anthropogenic nitrogen deposition over the northern Indian Ocean provided external reactive nitrogen that only weakly enhanced primary production (+10 mg $C.m^{-2}.d^{-1}.yr^{-1}$ in regions of intense deposition) and secondary production (+4 mg $C.m^{-2}.d^{-1}.yr^{-1}$). However, we find that locally this enhancement can significantly offset the declining trend in primary production over the last four decades in the central Arabian Sea and western Bay of Bengal, whose magnitude are up to -20 and -10 mg $C.m^{-2}.d^{-1}.yr^{-1}$ respectively.

KEYWORDS

atmospheric deposition, primary production, export, Indian Ocean, biogeochemical cycling, anthropogenic aerosols, nutrients, fertilization

1 Introduction

From 1980 to 2017, anthropogenic emissions of reactive N (Nr) in India have more than doubled (about +12 TgN.yr^{-1}). This change reflects an increase in both oxidized N emissions (NO$_x$ ≡ NO+NO$_2$, about +7 TgN.yr^{-1} equivalent to +300%), predominantly stemming from fossil fuel combustion, and NH$_3$ emissions (about +5 TgN.yr^{-1} equivalent to +80%), primarily originating from agriculture (McDuffie et al., 2020). In the atmosphere, Nr participates in many photochemical reactions that play a major role for air pollution before it is removed by wet and dry deposition. These photochemical processes also convert part of Nr to long-lived compounds such as peroxyacetylnitrate (PAN) or particulate ammonium and nitrate, which facilitates the transport of anthropogenic Nr from continental sources to the Indian ocean. Increasing Nr deposition over the Indian ocean is supported by observations of reactive nitrogen species and dry-deposition fluxes, which have consistently highlighted the northern Indian Ocean, particularly Indian coasts and the northern Bay of Bengal (BoB), as hot spots for atmospheric nitrogen deposition due to proximity to source emissions (Sarma et al., 2022; Singh et al., 2012; Srinivas et al., 2011; Srinivas and Sarin, 2013; Wiggert et al., 2006a).

The northern Indian Ocean has long been presumed N-limited (Morrison et al., 1998; Wiggert et al., 2005, 2006a; Lévy et al., 2007; Twining et al., 2019), suggesting potentially large integrated impacts of atmospheric nitrogen deposition on its productivity (Hamilton et al., 2023). However, it is important to acknowledge that the nutrient dynamics in the northern Indian Ocean is complex, variable in space and time and relatively poorly studied *in-situ*. Several observational and modeling studies (Morrison et al., 1998; Wiggert et al., 2005, 2006b; Koné et al., 2009; Twining et al., 2019; Thangaradjou et al., 2014; Hood et al., 2024) provide insights into the northern Indian Ocean productivity patterns and nutrient limitation, highlighting the key role of nitrogen limitation but also suggesting the potential role of co-limitations (e.g. nitrogen, phosphorus and iron in particular). Our understanding of how atmospheric nitrogen deposition contributes to biological production in the region remains limited, with most studies focusing on dust and iron deposition (Guieu et al., 2019; Patra et al., 2007b) and few model estimates available for the Bay of Bengal.

Concomitantly, Sridevi et al. (2023) observed between 2001 and 2020 a strong heterogeneity in the warming of the sea surface in the northern Indian Ocean influencing the rate of net primary production (NPP). Significant warming has been observed and a decline in productivity has been modeled south of 12°N, which are commonly attributed to decreased inputs of nitrogen from the subsurface ocean, either by reduced upwelling (off-Somalia) or increased stratification, and without accounting for atmospheric inputs (Roxy et al., 2016; Peng and Wang, 2024; Sridevi and Sarma, 2022). However, insignificant trends in NPP and warming were observed north of 12°N, associated with higher levels of anthropogenic aerosols (Sridevi et al., 2023). These trends suggest that the increasing deposition rate of nutrients from the aerosols could compensate for NPP declining trend due to warming in the northern Indian Ocean. Quantifying with an ocean biogeochemical model the balance between atmospheric deposition, which provides nitrogen, and warming, which restricts its supply by ocean circulation, becomes imperative for discerning accurately future spatio-temporal patterns of changes in the upper ocean biogeochemistry of the region.

In this study, we evaluate how much of the climate-driven productivity decline in the northern Indian Ocean is offset by the increase in N deposition, and quantify the efficiency of N deposition in driving additional productivity and carbon export below the surface layer (below 100 m depth). We address these questions with a state-of-the-art eddy-resolving ocean biogeochemical model of the Indian Ocean, forced either with increasing or fixed atmospheric N deposition, and quantify the change in primary production and export over the past four decades attributed to climate variability on the one hand, and to atmospheric N deposition on the other.

2 Materials and methods

The offset of primary production decline over the last forty years (1980-2020) in the northern Indian Ocean is evaluated with a set of three regional model simulations which are described below. The most realistic one captures the effects of climate variability on changes in ocean circulation and nutrient supplies, as well as the impact of increasing atmospheric deposition of nitrogen. In the second experiment, the external sources of nitrogen are kept constant at 1980s levels. The third one is a control experiment with both atmospheric forcing and deposition constant to 1980s levels. The comparison of the different simulations is then performed over the 40-year period (1980-2020) using trends to represent separately the effects of climate and of nitrogen deposition on primary productivity.

2.1 Ocean biogeochemical model

The simulations were conducted with the Geophysical Fluid Dynamic Laboratory (GFDL) Modular Ocean Model version 6 (MOM6) (Adcroft et al., 2019; Dunne et al., 2020) coupled to the ocean biogeochemical model Carbon, Ocean Biogeochemistry and Lower Trophics version 2 (COBALTv2) (Stock et al., 2020, 2014). We used an 'eddy resolving' regional configuration of the Indian Ocean with a 1/12° horizontal resolution (~8 km resolution), hereafter MOM6-COBALT-IND12. The methodology for the regional setup is similar to that used by Ross et al. (2023) in the Northwest Atlantic. MOM6-COBALT-IND12 covers the Arabian Sea, the Bay of Bengal and the equatorial Indian Ocean down to Java (32°E to 114°E and 8.6°S to 30.3°N, Figure 1). It includes 75 hybrid z*-isopycnal levels with z* coordinate near the surface (2-m layers at the surface) and a modified potential density coordinate below, identical to the hybrid z*-isopycnal developed in Adcroft et al. (2019).
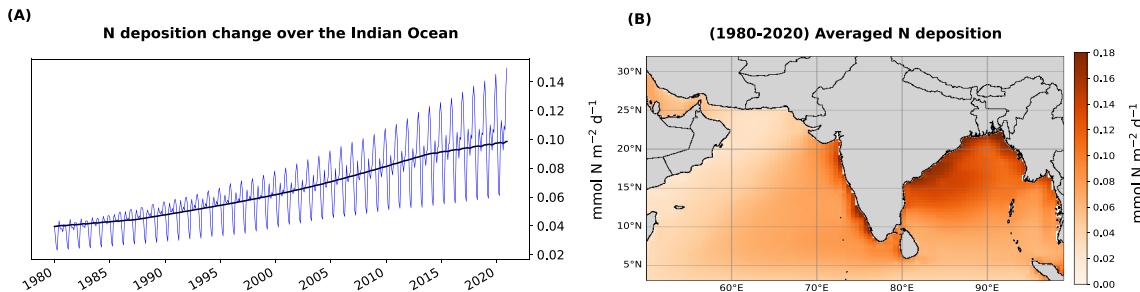
COBALTv2 integrates 33 tracers including three phytoplankton groups (small, large phytoplankton and diazotrophs), three zooplankton size classes (small, medium, large), the biogeochemical cycles of five limiting nutrients [nitrate (NO_3^-), ammonium (NH_4^+), phosphate (PO_4^{3-}), silica (silicic acid $Si(OH)_4$), and iron (Fe)], dissolved oxygen, carbonate species, three pools of dissolved organic matter, and particulate organic matter (Stock et al., 2020).

2.2 Atmospheric deposition

Dry and wet atmospheric deposition of Fe, lithogenic dust, PO_4^{3-}, NO_3^-, and NH_4^+ used to force the simulations were produced by the GFDL's Earth System Model Version 4.1 (ESM4.1, Dunne et al., 2020) published as part of the Coupled Model Intercomparison Project 6 (Eyring et al., 2016; O'Neill et al., 2016). ESM4.1 includes a detailed representation of anthropogenic and natural (e.g., biomass burning, lightning) reactive N emissions, photochemical processing, and removal by wet and dry deposition. ESM4.1 also includes an interactive representation of the land-atmosphere-ocean cycling of dust and ocean ammonia outgassing (Paulot et al., 2020; Horowitz et al., 2020).

Here, we use archived deposition fields from the historical run over the 1980–2014 period [1] and from the high emissions SSP5-8.5 scenario after 2015[2]. Historical and SSP5-8.5 anthropogenic emissions are from Hoesly et al. (2018) and Kriegler et al. (2017), respectively. Note that the choice of SSP5-8.5 has little influence on the results as the deposition between 2015 and 2020 are very similar in all the scenarios. The raw atmospheric deposition data, derived from ESM4.1, were processed to create atmospheric deposition forcing files for the ocean biogeochemical model spanning years 1980 to 2020. For dry and wet deposition of oxidized and reduced N, the objective was to retain the long-term trend and seasonality of the atmospheric deposition simulated by the ESM but remove interannual variability which is not in phase with the variability

that occurred in nature over the 1980-2020 period. This was achieved using a 15-year moving average by month that preserves the seasonal increasing trend. For Fe and PO_4^{3-} deposition, we used seasonal climatologies for the 1980-2020 period, i.e., there is no long-term trend or interannual variability. Fe deposition was directly taken from ESM4.1 outputs while PO_4^{3-} deposition was derived from the ESM4.1 climatology in dry lithogenic dust deposition, considering 563 ppm phosphorus content in dust, of which 22% is bioavailable (see values from global ocean averages of Herbert et al. (2018) and Ross et al. (2023)).

Atmospheric deposition over the northern Indian Ocean is strongly influenced by the seasonally reversing monsoonal winds (Singh et al., 2012; Gadgil, 2003; Shankar et al., 2002; Schott and McCreary, 2001), which blow from the northeast direction during the winter monsoon (November to February) and from the southwest direction during the summer monsoon (June to September). Patterns in atmospheric nitrogen deposition closely follow these monsoonal winds and precipitation. Over the northern Indian Ocean, dry deposition rates are linked to regional wind patterns, which modulate the loading of Nr within air masses and their trajectories. Notably, during the winter monsoon, higher deposition rates are observed in the eastern Arabian Sea (AS) attributed to northeast winds transporting aerosols from land to sea (Hamilton et al., 2023; Singh et al., 2012; Sarma et al., 2022). The 1980-2020 average dry deposition of nitrogen, obtained from the ESM4.1 model simulations, is 0.024 mmol $N.m^{-2}.d^{-1}$, comprising 77% oxidized and 23% reduced nitrogen. Conversely, wet deposition occurs through scavenging by clouds and precipitation, and is particularly prominent during the rainy summer monsoon in the Bay of Bengal (Jiang et al., 2021; Sinha et al., 2019). The estimated 1980-2020 average wet deposition of nitrogen in the northern Indian Ocean is 0.044 mmol $N.m^{-2}.d^{-1}$, with 45% oxidized and 55% reduced nitrogen.

2.3 Simulations and experimental protocol

Three simulations were conducted using the MOM6-COBALT-IND12 model to assess the influence of atmospheric N deposition and of climate variability (e.g., warming) on primary productivity and carbon export in the Indian Ocean. They were run from 1980 to

2020 using the hourly European center for medium-range weather forecasts reanalysis 5th generation (ERA5) atmospheric forcing e.g., wind, air tempearture and humidity, radiation, precipitation; (Hersbach et al., 2020). The simulations include explicit barotropic tidal momentum forcing based on the TPX09 product (Kriegler et al., 2017). River freshwater discharges in both simulations were sourced from the gridded daily Global Flood Awareness System (GloFAS) reanalysis version 4.0 (Harrigan et al., 2020). Riverine inputs of dissolved inorganic and organic nitrogen and phosphorus and particulate nitrogen were using the annual mean values (referenced to year 2000) from GLOBAL NEWS2 (Mayorga et al., 2010). The constant concentrations of DIC, alkalinity, and lithogenic minerals from river sources were allocated in both simulations, using the same values specified in Stock et al. (2020). The dissolved iron from rivers is set at a value of 70 nanomolar, according to Raiswell and Canfield, 2012. The open boundary conditions (OBCs) for temperature, salinity and velocity are derived from the monthly Ocean Reanalysis System (ORAS5) product (Zuo et al., 2019). OBCs for nitrate, phosphate, silicate, and oxygen are based on monthly climatologies from the World Ocean Atlas 2018 (Boyer et al., 2018) and OBCs for dissolved inorganic carbon (DIC) and alkalinity are based on annual mean values from GLODAPv2 (Olsen et al., 2016). Simulations were started after a 32-year spin-up achieved by looping four 8-year 1980-1987 forcing loops.

The first simulation, includes the effect of both climate change and nitrogen deposition and is referred to as the CC-NDEP experiment. CC-NDEP represents the evolution from 1980 to 2020 for the atmospheric forcing and the atmospheric deposition of dry and wet nitrogen (NO_3^-, and NH_4^+), phosphate (PO_4^{3-}), lithogenic dust, and iron (Fe). The second simulation, isolates the effect of climate change and is termed the CC experiment. CC sets the atmospheric nitrogen deposition constant to 1980 levels while maintaining the evolution of the atmospheric forcing and the deposition of lithogenic dust, phosphate and iron identical to the CC-NDEP experiment. The third experiment represents a control simulation referred to as the CTRL with constant atmospheric forcing and deposition using a loop from 1980-1987 of the CC-NDEP experiment. We define the 'Climate change response' as the CC experiment and the 'Nitrogen deposition change response' as the difference between the CC-NDEP and CC experiments. We focus the analysis on the northern Indian Ocean (3°-32°N, 50°-100°E), AS (3°-32°N, 50°-78°E) and BoB (3°-32°N, 78°-100°E), (Figure 1B).

2.4 Trend analysis and export efficiency

We use in our study the spatial trends over the 1980-2020 period calculated using simple linear regression with 95% confidence interval to estimate the effects of climate and N deposition on the northern Indian ocean biogeochemistry. The trend of CC-NDEP minus the trend of CC corresponds to that of the 'Nitrogen deposition change response', and the trend of CC to the 'Climate change response'. The CTRL simulation showed no

significant trend in the Northern Indian Ocean, suggesting that the model drift is small.

We also estimate the export efficiency for these two responses, computed as the ratio of exported organic carbon at 100 meters to primary production, integrated over the 1980-2020 period for the northern Indian ocean. The comparison between these ratios determine which response has the largest effect over the period. A higher export efficiency for the 'Nitrogen deposition change response' than for the 'Climate change response' suggests that the additional primary production driven by the N deposition leads to more export in deep waters compared to the primary production driven by climate change.

2.5 Observations

We evaluate the MOM6-COBALT-IND12 model against observation-based upper ocean stratification and satellite-derived biogeochemical fields. We used the annual climatology of temperature and salinity, obtained from World Ocean Atlas 2018 (WOA18)[3] (Locarnini et al., 2018; Zweng et al., 2019), to compute upper-100m-averaged buoyancy frequency (N^2), with a resolution of 0.25°×0.25°. We used the observation-based monthly climatology of mixed layer depth (MLD) at 1°×1° spatial resolution, calculated with a fixed threshold criterion (0.03 $kg.m^{-3}$) in density (de Boyer Montégut et al., 2004), obtained from the SEANOE website[4]. Satellite-based monthly chlorophyll concentrations with a resolution of 4 km, derived by SeaDAS using a blended combination of OCI (OC4v6 + Hus CI), OC3, and OC5 algorithms contingent upon water class memberships (Sathyendranath et al., 2019), were obtained from the ESA Ocean Colour Climate Change Initiative (OC-CCI v5.0) website[5]. Satellite-based net primary productivity, also computed monthly with a resolution of 1/6°, relies on the updated Carbon-based Production Model (CbPM) algorithm developed by Westberry et al. (2008), accessible via the Ocean Productivity website[6]. All satellite-based data was regridded to a resolution of 0.25°×0.25°.

3 Results

After presenting the atmospheric N deposition patterns (Figure 1), and then evaluating the model (Figure 2) and its declining trend in productivity over the recent period, we explore how atmospheric N deposition could act as a compensatory

---

fertilizing mechanism counterbalancing the decline in productivity tied to climate change. To distinguish the influence of the atmospheric N deposition from that of climate variability, the 'Climate change response' and 'N deposition change response' for primary production, secondary production, carbon export below 100 m depth and surface chlorophyll concentration are evaluated separately (Figures 3–5). Finally, the efficiency of N deposition in driving additional production and export is evaluated (Figure 6).

3.1 Characterization of atmospheric N deposition

Atmospheric N deposition simulated by the GFDL atmospheric model has significantly increased in the Indian Ocean over the past four decades (Figure 1A). The mean N deposition from 1980 to 2020 exhibits a pronounced east-west gradient in the AS and north-south gradient in the BoB (Figure 1B). Notably, substantial deposition rates
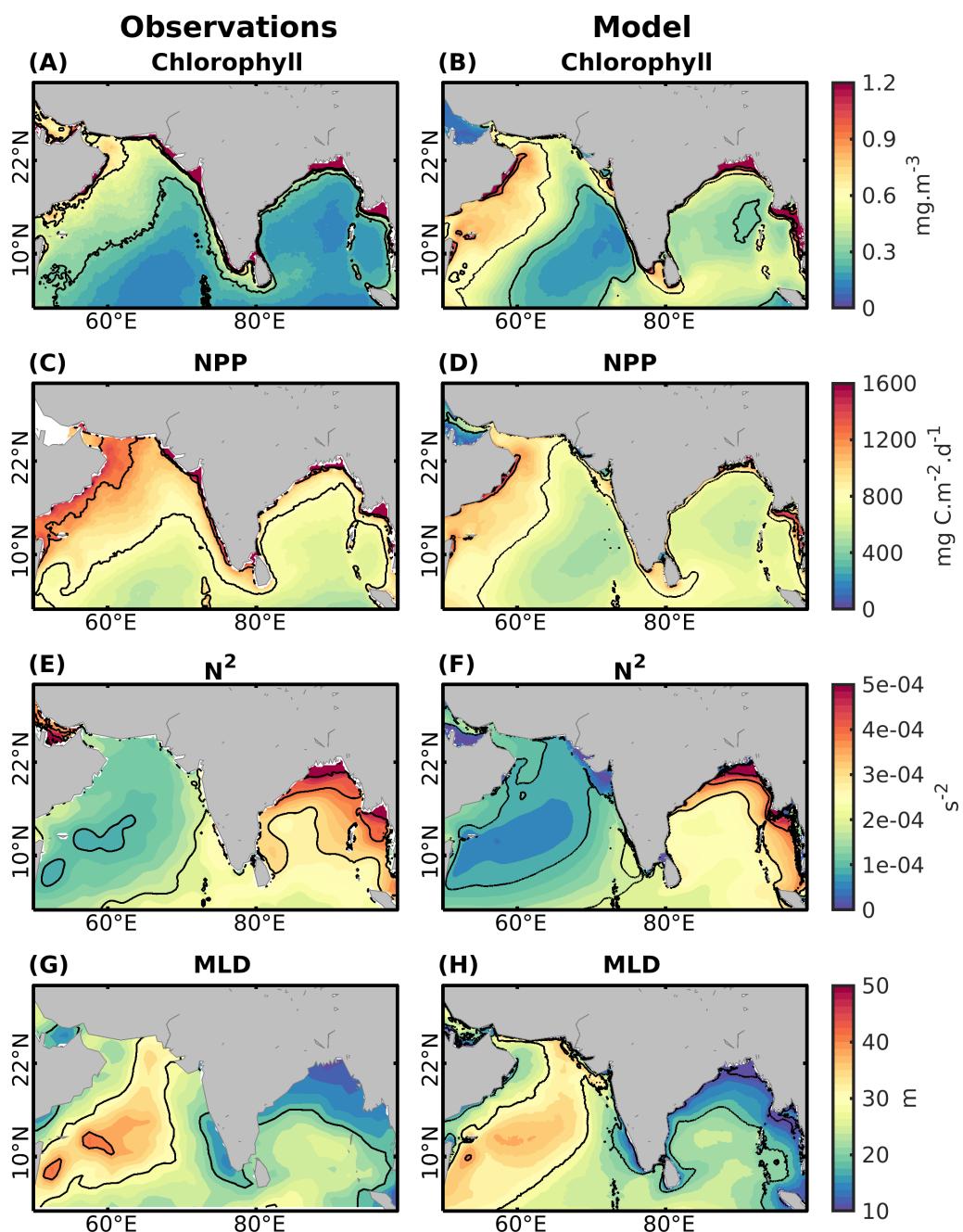
FIGURE 2
Comparison of observation-based and modelled ocean properties in the northern Indian Ocean. Left column: observation-based estimates of **(A)** surface chlorophyll ($\mu g.kg^{-1}$), **(C)** 0-100m integrated net primary production (NPP, $mgC.m^{-2}.d^{-1}$), **(E)** 0-100m averaged squared buoyancy frequency (N^2, s^{-2}), and **(G)** mixed layer depth (MLD, m). Right column: same as left column, but for output from the CC-NDEP simulation **(B, D, F, H)**. Black contours indicate specific values corresponding to the levels shown on each colorbar. Surface chlorophyll and NPP were averaged over the observation period 2003-2020. N^2 and MLD were averaged over 1980-2020. The observational products used for each variable are given in the Material and methods.

are found in the northern BoB and eastern AS (0.2 mmol N.m^{-2}.d^{-1} along the coasts of India, Bangladesh and Myanmar) going down to much lower values in the western AS and southern BoB (0.02 mmol N.m^{-2}.d^{-1}). Moreover, the time series of atmospheric N deposition reveals a clear upward trend in total N deposition (NIO: 0.0017, AS: 0.0015, BoB: 0.002 mmol N.m^{-2}.d^{-1}.yr^{-1}) with decreasing trends in total N deposition from the coasts to offshore areas (0.25 to 0.05 mmol N.m^{-2}.d^{-1} (see Supplementary Figure S3). A progressive increase in the amplitude of the seasonal cycle of deposition is observed in the northern Indian Ocean throughout the period 1980-2020 reaching +0.068 mmol N.m^{-2}.d^{-1} (Figure 1A). These spatial gradients arise from the interplay between seasonal reversals of monsoonal winds, precipitation patterns and location of continental emission sources. In summer, deposition peaks in the northern BoB and in the coastal eastern AS where southwesterly winds can carry aerosols originated from land and precipitation is most intense (see Supplementary Figure S1). In winter, deposition is more homogeneous over the northern Indian Ocean due to lower precipitations and northeasterly winds that blow over the continent before reaching the open ocean (see Supplementary Figure S1).

While observational estimates of total N deposition are not available for the region, Sarma et al. (2022) provide estimates of the dry component of N deposition. The strong spatial gradients in dry N deposition simulated by the atmospheric model in the AS and BoB (see Supplementary Figure S2) agree with the observation-based estimates. Our estimate of mean dry N deposition over the northern Indian Ocean between 2001 and 2020 varies spatially between 0-1.8 mg N.m^{-2}.d^{-1}, similar to the range derived from anthropogenic aerosol measurements by Sarma et al. (2022) (0-2.1 mg N.m^{-2}.d^{-1}). The atmospheric model and observation-derived product depict similar gradients across the AS and BoB, presenting higher fluxes along the eastern AS and northern BoB coastal regions. However, they estimated the deposition of atmospheric inorganic nitrogen over the entire AS and BoB over the (2001-2020) period to be 1.7 +/- 0.4 and 0.9 +/- 0.2 TgN yr^{-1} respectively, which magnitudes are higher than our N dry deposition trends simulated by the ESM for the same period (AS: 0.47; BoB: 0.32 TgN yr^{-1}).

3.2 Model evaluation of primary productivity and upper ocean stratification

In this section, we evaluate the climatological mean over the 2003-2020 period for surface chlorophyll and net primary production (NPP) in the model simulation (CC-NDEP) against estimates from satellites and *in-situ* observations, as well as the mean state of upper ocean stratification (mixed-layer depth MLD, and buoyancy frequency N^2 averaged in top 100 m, Figure 2).

The model reproduces the mean observed patterns of upper ocean dynamics, including the strong AS-BoB contrast characterized by lower stratification and deeper MLDs (down to 40 m) in the central AS and highly stratified and very shallow MLDs in the northeast BoB (Figures 2E, F). These distinct physical regimes dictate the pattern in productivity by controlling the nutrient supply and phytoplankton bloom dynamics (Wiggert et al., 2005, 2006a). In the AS, summer-monsoon upwelling along the Arabian Peninsula and southwest Indian coast and winter-monsoon convective mixing in the northeastern AS facilitate nitrogen supply to the surface. This supply of nitrogen, along with the iron delivery from Arabian dust deposition, fuels intense productivity (Jickells et al., 2005; Resplandy et al., 2011; Singh et al., 2012). Conversely, the BoB exhibits lower productivity, primarily because freshwater-induced stratification inhibits the supply of nutrients by coastal upwelling and vertical mixing (higher N^2 and shallow MLD, Figures 2E–H), except at the mouths of the Brahmaputra and Ganges rivers where nutrients discharge is important during the rainy summer monsoon (Kumar et al., 2004; Lévy et al., 2007; Prakash and Ramesh, 2007; Singh and Ramesh, 2011; Singh et al., 2012).

We assess the model results by comparing surface chlorophyll concentration and depth-integrated NPP in the CC-NDEP simulation to satellite-based products averaged over the 2003-2020 period (Figure 2). The model reproduces the observed contrast of high surface chlorophyll concentrations in the coastal upwelling systems of Oman and southern India and along the coast of Bangladesh and Myanmar (>1.2 mg.m^{-3}) down to the very low values offshore in the southern AS and central BoB (<0.2 mg.m^{-3}, Figures 2A, B). Patterns of modelled NPP are also consistent with the distribution of remote-sensing-based estimates in each basin, capturing elevated values reaching 1000 mg C.m^{-2}.d^{-1} along the coasts of Oman, Bangladesh, Myanmar and at the major Indian deltas (Figures 2C, D). Our model estimates of NPP in the upper 5 m over the 1994-2019 period reach 800 mg C.m^{-2}.s^{-1} along the northern Indian Ocean coasts and 0-350 mg C.m^{-2}.d^{-1} in the open ocean. This latter falls within the range of values measured during campaigns in the northern Indian Ocean between 1994 and 2019, with estimates in the AS ranging from 7.8 to 387 mg C.m^{-2}.d^{-1} and in the BoB ranging from 6.8 to 225 mg C.m^{-2}.d^{-1} (Sarma et al., 2022).

The model tends to simulate higher surface chlorophyll concentrations but lower NPP than those observed in the central AS and southern BoB (Figures 2B, D). These systematic differences likely arise from a combination of model biases, included in the representation of the chlorophyll to carbon ratio and its sensitivity to iron concentrations and light levels, and uncertainties in the algorithms used to reconstruct surface chlorophyll and primary productivity from satellite images, particularly in the Indian Ocean (Kalita and Lotliker, 2023). It also highlights the well-known limitation of using chlorophyll as a proxy for NPP. Nevertheless, we are confident that the simulations capture the main patterns of productivity in the region.

We further evaluate the temporal change in modelled primary production over the 1980-2020 period (Figure 3B). It suggests that phytoplankton productivity has declined in the northeastern AS and the central BoB (e.g., primary production decline of -10 mg C.m^{-2}.d^{-1}.yr^{-1}), but has insignificant trends elsewhere. Trend in primary production obtained from satellite observations covering the 2003-2020 period are not significant in the northern Indian Ocean (not shown), likely due to the short period and high interannual variability. We find, however, that the trends in our model agree with the trends found in the Copernicus Marine Environment Monitoring Service (CMEMS) high-resolution
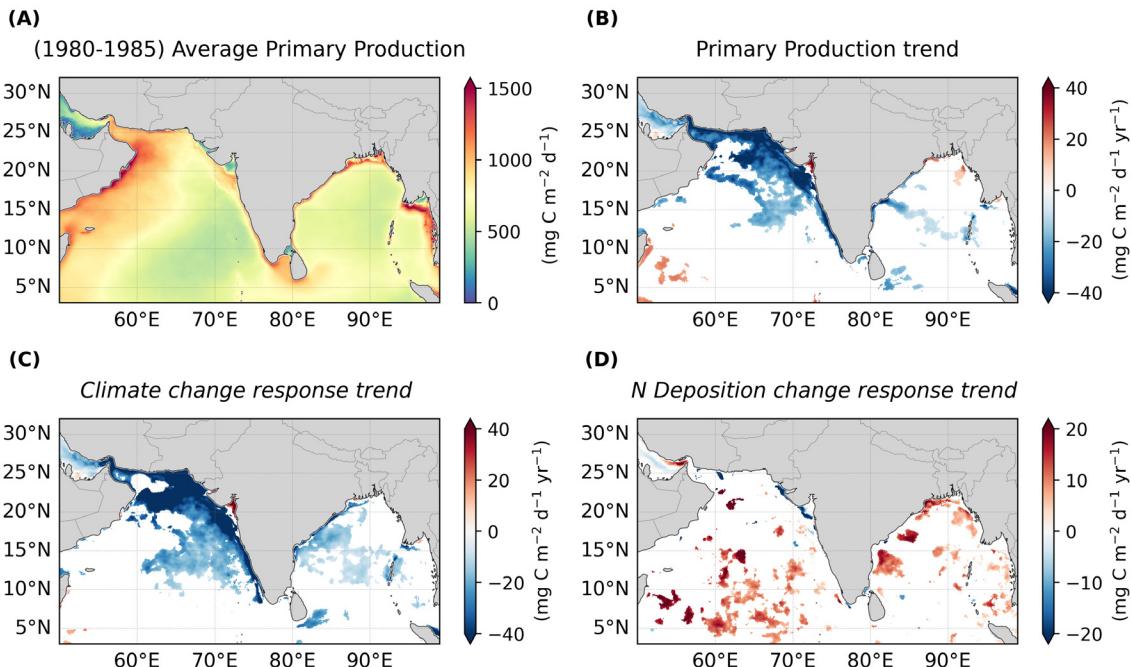
FIGURE 3
Simulated baseline state and trend contributions in the northern Indian Ocean primary production: total contribution, negative contribution due to climate change and positive contribution due to N deposition change. **(A)** Primary production integrated in top 100m averaged over 1980- 1985 for CC-NDEP simulation ($mgC.m^{-2}.d^{-1}$), **(B)** its trend over 1980-2020 in CC-NDEP experiment ($mgC.m^{-2}.d^{-1}.yr^{-1}$), **(C)** its 'Climate change response' trend over 1980-2020 in the CC experiment and **(D)** 'N deposition change response' trend over 1980-2020 in the (CC-NDEP minus CC) experiment. The masking regions indicate no significant trends ($p > 0.05$).
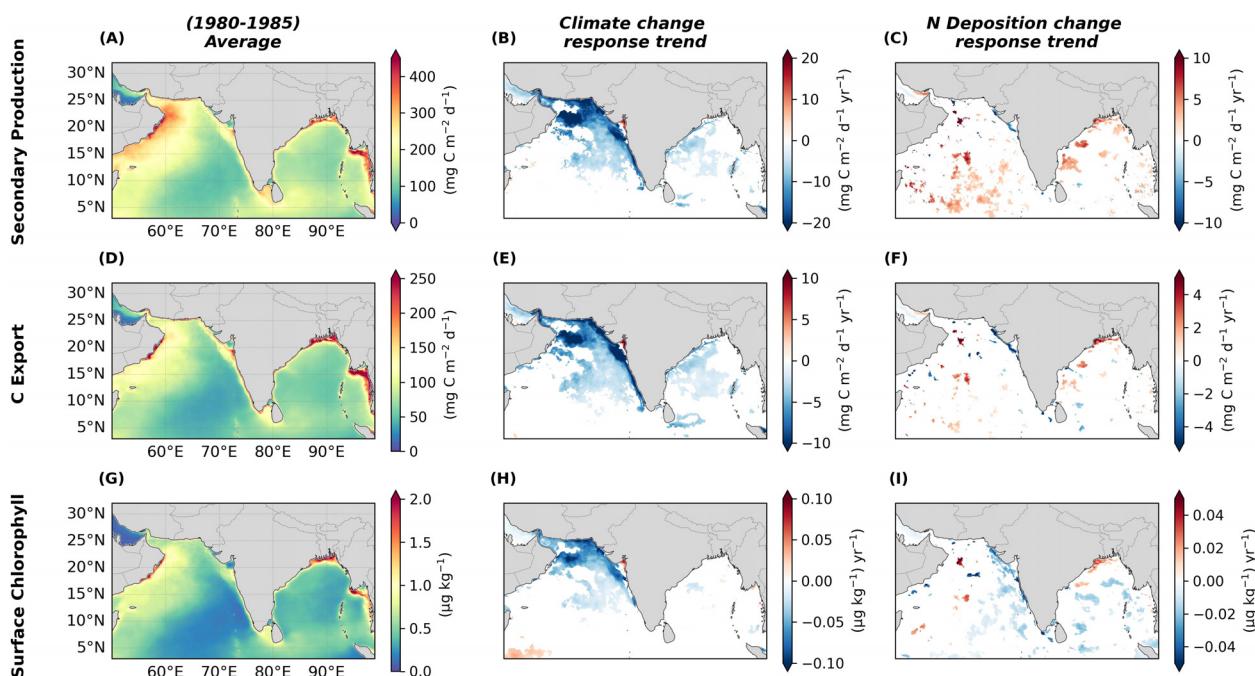
FIGURE 4
Simulated baseline state and trend contributions in the northern Indian Ocean secondary production, C export, and surface chlorophyll.
(A) Secondary production integrated in top 100m, **(D)** C export at 100m ($mgC.m^{-2}.d{-1}$) and **(G)** surface chlorophyll concentration ($µg.kg^{-1}$) averaged over 1980-1985 for CC-NDEP simulation, their 'Climate change response' trend **(B, E, H)** and 'N deposition change response' trend **(C, F, I)** over 1980-2020. The masking regions indicate no significant trends ($p > 0.05$).
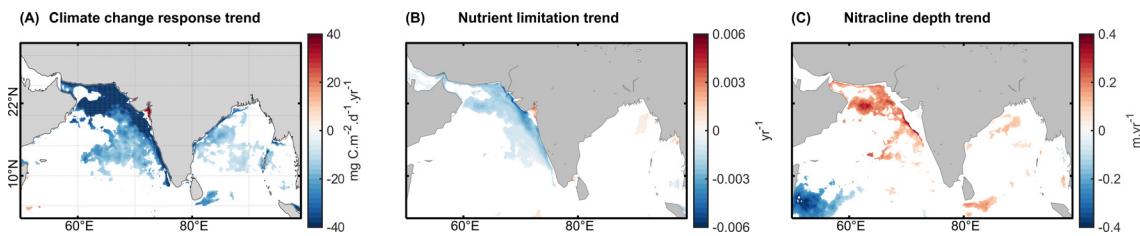
FIGURE 5
Climate change response trend in the northern Indian Ocean primary production associated with reduced upward nutrient fluxes. **(A)** 'Climate change response' trend for primary production over 1980-2020 ($mgC.m^{-2}.d^{-1}.yr^{-1}$). **(B)** Surface layer nutrient limitation trend (yr^{-1}) and **(C)** nitracline depth trend ($m.yr^{-1}$) in the northern Indian Ocean over 1980-2020 responding to climate change response. The nitracline corresponds to the depth where NO_3^- concentration reaches 1 µmol.kg−1 and has been obtained by vertically interpolating NO_3^- concentration into 1-m resolution for the upper 200 m. The masking regions indicate no significant trends ($p > 0.05$).

reanalysis data[7] used in Maishal (2024), which show a decline in primary production (-1.0 to -2 mg $C.m^{-3}.d^{-1}.yr^{-1}$) in the northern Indian ocean over the period 1998-2022.

3.3 Climate change response

The impact of climate variability on the biogeochemistry of the Indian Ocean is evaluated by measuring the temporal change in productivity (primary production, secondary production, carbon export, surface chlorophyll) over the 1980-2020 period in the climate change (CC) experiment. First we describe the general patterns in the 1980s (Figures 3A, 4A, D, G) and then the climate change response trends (Figures 3C, 4B, E, H).

Primary productivity integrated over the upper 100 m shows zones of intense productivity, with values exceeding 1000 mg $C.m^{-2}.d^{-1}$, particularly evident in upwelling regions such as the western AS (Figure 3A). These zones of intense productivity coincide with regions exhibiting significant secondary zooplankton production (exceeding 250 mg $C.m^{-2}.d^{-1}$) and carbon export below 100 m depth (exceeding 100 mg $C.m^{-2}.d^{-1}$). Lowest productivity and export patterns are observed in the southeastern AS and central BoB where nutrient supply by ocean dynamics is low and N limitation is high.

The climate change response is characterized by decreasing trends in primary production, secondary production and export production reaching respectively around -20, -5 and -2 mg $C.m^{-2}.d^{-1}.yr^{-1}$ in the eastern AS and western BoB (Figures 3C, 4B, E, H), with significant trends reaching -40, - 20 and -10 mg $C.m^{-2}.d^{-1}.yr^{-1}$ found in the coastal eastern AS. To identify the drivers of this decreased productivity associated with the climate change response, we examine the temporal change in surface layer nutrient limitation and the nitracline depth over the 1980-2020 period in the CC simulation (Figure 5). The nutrient limitation represents the Liebig's nutrient limitation factor, calculated as the minimum of nitrogen limitation (including NO_3^-, and NH_4^+), phosphorus limitation, and iron deficiency, and the nitracline depth is representing the NO_3^- concentration at 1 µmol.kg−1. The eastern AS exhibits a reduced

vertical nutrient supply along the Indian coast and offshore that is characterized by a stronger limitation with a significant decrease in the nutrient limitation coefficient up to -0.002 yr^{-1} coupled to an increase of the nitracline depth of +0.2 $m.yr^{-1}$. In the BoB, changes consistent with reduced vertical nutrient supply are not significant. Nevertheless, increased nutrient limitation in the AS dominates the 'Climate change response' signal. Hence, these findings suggest that the decline in productivity in the 'Climate change response' could be attributed to reduced vertical nutrient supply associated with the deepening of the nitracline, likely in response to upper ocean warming and enhanced stratification, as previously reported in low-latitude oceans due to global warming (Duce et al., 2008; Sarma et al., 2022; Roxy et al., 2016).

3.4 Nitrogen deposition change response

The impact of increasing N deposition on the biogeochemistry of the Indian Ocean (Figures 3D, 4C, F, I) is evaluated by measuring the temporal change in mean productivity (PP, secondary production, carbon export, surface chlorophyll) over the 1980-2020 period in the (CC-NDEP minus CC) experiment which enables us to remove the climate effect.

We can first note that areas of naturally low productivity remarkably coincide with areas experiencing intense N deposition in the Indian open ocean (Figures 1B, 3A). This correspondence suggests a potentially significant effect of N deposition in these regions naturally characterized by limited N supply. We find that the N deposition effect leads to increasing trends in primary production (+10 mg $C.m^{-2}.d^{-1}.yr^{-1}$), secondary production (+4 mg $C.m^{-2}.d^{-1}.yr^{-1}$) but insignificant ones for export in regions of intense deposition in eastern AS and northern BoB. This contrasts with a decrease in surface chlorophyll (about -0.01 $\mu g.kg^{-1}.yr^{-1}$) in the same area of the eastern AS. As shown in the next section, this decrease in surface chlorophyll despite the increase in primary production is explained by the simulated increase in small phytoplankton (with lower chlorophyll to carbon ratio) at the expense of large phytoplankton (with higher chlorophyll to carbon ratio), in addition to grazing pressures from increased secondary production. These results suggest the fertilization effect of atmospheric N deposition at the basin-scale.

7 https://data.marine.copernicus.eu/products.
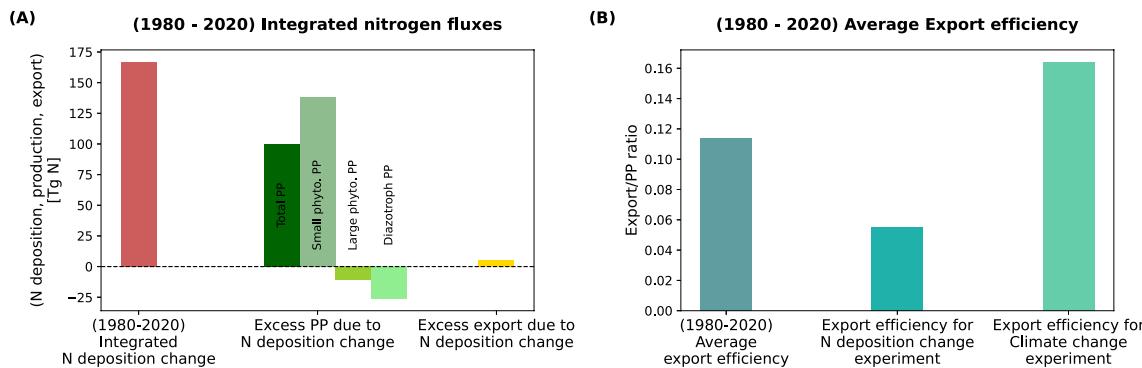
FIGURE 6
Integrated and averaged impact of nitrogen deposition change on primary production, export and export efficiency (1980-2020). **(A)** Total change in total primary production (dark green, TgN) and in export (yellow, TgN) in response to total N deposition change integrated from 1980 to 2020 (pink, TgN). Integrated changes in small phytoplankton, large phytoplankton and diazotroph biomasses to total change in primary production are also represented (light green bars, TgN). **(B)** Export efficiency calculated as export to primary production ratio averaged from 1980 to 2020 for the CC-NDEP experiment, and for the 'N deposition change response' experiment (CC-NDEP minus CC) and 'Climate change response' experiment (CC minus CTRL).

The declining trend in primary production due to climate change affects broader regions than the trend due to nitrogen deposition change and likely represents the dominant factor influencing the northern Indian Ocean's primary production (Figures 3C, D). Yet, the effect of nitrogen deposition change offsets that of climate change in the central Arabian Sea and the western Bay of Bengal by more than 70% and 100% respectively. While these areas of significant trends are limited, the increase in nitrogen deposition appears to have a notable local impact in compensating climate-driven declines in productivity.

3.5 Efficiency of nitrogen deposition for production and export

Here we examine whether N deposition is efficiently utilized, i.e. how much of N deposition is used to increase primary production and export. We find that the total surplus in primary production due to N deposition is more than half of the total increase in N deposition between 1980 and 2020, with 100 out of a total 167 Tg N from N deposition used for primary production (60%, Figure 6A), confirming that N deposition is efficiently used by phytoplankton. In contrast, we find that the increase in export associated with the N deposition is almost negligible, with only 5.5 out of 167 Tg N exported (Figure 6A). This is because the additional N favors small phytoplankton production (equivalent to +138 Tg N) that contributes less to export, at the expense of a decline in large phytoplankton production (-11 Tg N, Figure 6A). As a result, the export efficiency associated with atmospheric N deposition of 5.5% is much lower than the total export efficiency of the system of 11% and the export efficiency associated with the climate change response of 17% (Figure 6B).

While N deposition promotes small phytoplankton production and total primary production, it does not manifest as a net increase in the surface chlorophyll; instead, it drives a decrease in surface chlorophyll (-0.01 μg.kg^{-1}.yr^{-1}, Figure 4I) as the average chlorophyll to carbon ratio of the phytoplankton community decreases. This

discrepancy between primary production and chlorophyll trends highlights the challenge of estimating trends in primary production from ocean color. To compound this effect, N deposition directly contributes to the enhancement of secondary production, with an increase exceeding +4 mg C.m^{-2}.d^{-1}.yr^{-1} (Figure 4C), which is likely to further drive down surface chlorophyll from increased zooplankton grazing rates.

4 Discussion

4.1 Comparison to previous work

Since the seminal work of Duce et al. (2008) over 15 years ago, atmospheric nitrogen deposition, whose levels are increasing due to anthropogenic disturbances, is increasingly recognized as a long-term, low-level fertilization mechanism for marine productivity, with significant implications for natural biogeochemical cycles (Hamilton et al., 2023).

In the northern Indian Ocean, recent studies have documented a significant increase in nitrogen deposition loads over 2001-2020 (Sarma et al., 2022) and have investigated the potential impact of this increase on marine productivity (Sarma et al., 2020; Bikkina et al., 2021; Srinivas and Sarin, 2013; Sridevi and Sarma, 2022). Through microcosm experiments where aerosol samples were mixed with coastal waters from the Bay of Bengal, Yadav et al. (2016) and Kumari et al. (2022a) estimated that soluble nitrogen deposition could enhance primary production by 3-33% and 3-19%, respectively. Note that these microcosm experiments focus on the surface layer and are conducted in coastal regions where nitrogen deposition and phytoplankton response are high. Our modeling results, which consider the photic zone production over the entire basin, identify atmospheric nitrogen deposition hot spots along the coasts of India, Bangladesh, and Myanmar, resulting in increases in primary production of +10 mg C.m^{-2}.d^{-1}.yr^{-1} over the past four decades. The discrepancy in percentage impact between microcosm experiments and model observations might be partly explained by

the fact that the model integrates the response over a broader spatial and vertical scale, including areas with lower deposition and phytoplankton response. It is also noteworthy that some of these regions are within the northern Indian Ocean Oxygen Minimum Zone (OMZ), where surface waters exhibit low N/P values due to upwelling of denitrified waters, suggesting enhanced nitrogen limitation in these areas.

Locally, the decreasing trend in primary production between 1980 and 2020 due to climate change can significantly be offset by the increasing trend in atmospheric deposition of inorganic nitrogen, with compensation reaching over 100% in some regions of the western Bay of Bengal and 70% in the central Arabian Sea. As discussed later in the 'Limits' section, this study does not account for the role of dissolved organic nitrogen deposition, which could further enhance this compensatory effect, as studies have shown that dissolved organic nitrogen can be efficiently utilized by phytoplankton (Sipler and Bronk, 2015; Sarma et al., 2019). Therefore, the impact of atmospheric nitrogen deposition on mitigating the decline in primary production is likely greater than estimated here.

On a larger scale, and assuming that deposited nitrate and ammonium were fully utilized by phytoplankton with a C/N ratio of 6.6, Sarma et al., 2022 estimated the contribution of atmospheric deposition of inorganic nitrogen to primary production in the entire BoB and AS at 14 ± 7% and 11 ± 8%, respectively. These estimates are considerably higher than the results of our estimations indicating that the total atmospheric N deposition has contributed to supporting 100 Tg N for primary production within the top 100 m in the NIO (Figure 6A), representing approximately 0.6% of the total primary production over the 1980-2020 period (17270 Tg N). However, it is important to note that Sarma et al., 2022 derived these values using primary production confined to the uppermost ocean layer (5m) over the 2001-2020 period and for dry deposition only. By calculating this contribution based on our simulations but restricting the primary production estimation to the uppermost layer over the 1980-2020 period, the obtained result (0.3% for NIO) is still lower than previous findings.

Regarding the contribution of N deposition to export production, however, our results differ significantly from previous estimations. Indeed, most studies assume that the deposition-induced increase in NPP directly contributes to export [e.g., Sarma et al., 2022, assume that new production, supported by atmospheric deposition, contributes to ∼ 17% and 6% of export production to the oxygen minimum zone in the BoB and AS, respectively]. On the contrary, we demonstrate that only a limited fraction of the increase in primary production translates into an increase in export (5.5% for the NIO, Figure 6B). This is largely explained in our simulations by the fact that the increase in primary production primarily occurs through an increase in nanophytoplankton primary production, coupled with a subsequent decrease in diatom-related primary production. As small phytoplankton export organic matter less efficiently than diatoms, this shift leads to more nutrient recycling within surface waters and more primary production based on regenerated nutrients.

In addition, our simulated fertilization effect of N deposition results in a shift from primary to secondary production, stimulating zooplankton growth and consequently reducing the surface chlorophyll signal. This observed effect on secondary production has not been previously demonstrated, and it contrasts with the rare increases in surface chlorophyll-a associated with atmospheric aerosol deposition like dust observed in the NIO by [Guieu et al. (2019); Patra et al. (2007a); Banerjee and Prasanna Kumar (2014); Lachkar et al. (2021)].

Our estimations indicate that the total atmospheric N deposition of 167 Tg N (average: 1.65 Tg N.yr^{-1}) has contributed to supporting 100 Tg N and 570 Tg C of primary production within the top 100 meters in the NIO. This contribution represents approximately 0.6% of the total primary production over the period and averaged over the region. Therefore, while atmospheric N deposition plays a role in compensating for climate-induced declines in primary production over the past decades, its overall impact appears to be limited. This finding is consistent with the results reported by Singh et al. (2012), who estimated that the contribution of atmospheric deposition to new production in the northern Indian Ocean could at best be around ~3%.

4.2 Limits/Caveats

Nitrogen atmospheric deposition fields used in our study are derived from an Earth System Model (ESM) simulation, which introduces a notable limitation regarding the consistency of the wind regime. Specifically, there is a lack of synchronization between the simulated wind patterns of the ESM and the reanalysis winds employed to force the physical component of our coupled system. This discrepancy arises from the difficulty in accurately capturing regional atmospheric dynamics at a finer scale.

We note that the rate of increase in anthropogenic aerosol optical depth has not been uniform over the past two decades. In the northern Bay of Bengal, for example, the increase has slowed in the past decade compared to earlier periods (Yadav et al., 2021). The accuracy of Nr emissions data for the Indian subcontinent remains uncertain, posing challenges for their utilization in models. For instance, the seasonality of ammonia (NH$_3$) emissions in this study is inconsistent with satellite observations, which could have implications for the transport of Nr to the Indian Ocean (Beale et al., 2022).

In addition, our study does not incorporate organic nitrogen in the deposition forcing. The omission of the representation of organic nitrogen sources and soluble organic nitrogen contributions may lead to an underestimation of the total atmospheric reactive nitrogen deposited to the northern Indian Ocean. Addressing this limitation requires further research to improve the representation of organic nitrogen sources in atmospheric deposition models. Moreover, the bioavailability of nitrogen resulting from atmospheric deposition remains a complex and challenging aspect to quantify accurately (Altieri et al., 2021; Hamilton et al., 2023, 2020; Kanakidou et al., 2016). Our study acknowledges the importance of considering the various forms of deposited nitrogen and their potential utilization by marine organisms, but uncertainties in bioavailability rates persist. The

dominance of smaller phytoplankton in response to nitrogen deposition in our results should be therefore interpreted with caution as the proportions of ammonium and soluble organic nitrogen in the total nitrogen deposition are not included in our analysis. This can drive community shifts by influencing the N/P ratio of the water-column and calls for further studies to comprehensively understand these dynamics (Jiang et al., 2021; Yuan et al., 2023).

In our simulations, the tendency of atmospheric iron deposition is held constant, whereas previous studies have highlighted the significant increase in iron emissions from industrial and natural sources due to anthropogenic combustion and land use changes over the Industrial Era, particularly in the global and Arabian Sea (AS) biogeochemistry (Guieu et al., 2019; Patra et al., 2007b; Sarma et al., 2022; Hamilton et al., 2023, 2020). By not accounting for this effect, our results may not fully capture the contribution of the increase in biomass of large phytoplankton, particularly diatoms, which have a higher Fe:C ratio and are known to export more organic matter than small phytoplankton. We would anticipate a stronger oceanic biological response over the study period if we were to consider this factor. Additionally, the evolution of iron deposition over the contemporary period could have implications for Fe-limited diazotrophs' contribution to export, denitrification, and the increase in nitrogen fixation, as modeled in the oligotrophic Arabian Sea by Hamilton et al. (2020). Incorporating these dynamic changes in iron deposition into future simulations could provide a more comprehensive understanding of its role in shaping biogeochemical processes and ecosystem dynamics in the northern Indian Ocean.

To accurately quantify the northern Indian Ocean response to atmospheric N deposition, it is imperative to gain a deeper understanding of how other external sources of nitrogen, such as nitrogen fixation and riverine nitrogen input, contribute to the ocean's nitrogen budget. For instance, N-budget for the northern Indian Ocean from [Srinivas and Sarin (2013); Sarma et al. (2022)] suggests that riverine supply is of comparable magnitude with atmospheric deposition supply with significant disparities between AS and BoB basins. Keeping the average external input of nitrogen from rivers constant to 2000 levels in our simulations captures an average input over the period, but lacks the increase in riverine nutrient inputs over the 1980-2020 period in the Bay of Bengal (Pedde et al., 2017), and might conceals potential impacts, such as eutrophication, which are not explicitly addressed in this study (Mayorga et al., 2010; Pedde et al., 2017; Suntharalingam et al., 2019; Sridevi and Sarma, 2022).

Additionally, our study exclusively examined nutrient deposition and does not address the effects of acidification resulting from atmospheric deposition. As noted in the studies of Sarma et al. (2015) and Kumari et al. (2021, 2022b), this indirect acidification can also enhance primary production. We recommend that future studies incorporate both nutrient deposition and acidification effects to provide a more comprehensive understanding of the impacts of atmospheric deposition on NPP.

Future trends in atmospheric N deposition and warming in the region remain uncertain with studies projecting an increasing atmospheric nitrogen deposition (Jickells et al., 2017) or modeling

a non-uniform warming of the northern Indian Ocean (Sharma et al., 2023). Assessing the future combined effects of nutrient deposition and climate change will require dedicated ocean-atmosphere coupled modeling studies that integrate both factors.

4.3 Potential implications for Oxygen Minimum Zones

The northern Indian Ocean hosts one of the most intense Oxygen Minimum Zones (OMZ) globally, characterized by oxygen concentrations in the AS and BoB reaching hypoxic levels (O2 <60 $\mu mol.kg^{-1}$), thereby impacting marine habitats. Atmospheric deposition over the OMZ surface supplies external nitrogen, enhancing biological production and facilitating the export of organic matter from surface layers to intermediate waters. This influx of nitrogen is likely to stimulate biological respiration, consuming oxygen and subsequently reducing its concentration in subsurface and intermediate waters. Given that oxygen levels in the OMZ are linked to the balance between biological production export and oxygen supply from intermediate water ventilation, the total 'N deposition change' in recent decades may have contributed to the intensification and extension of the OMZ (Sarma et al., 2022). While changes in export production may influence oxygen levels within the OMZ, our model results suggest that the magnitude of this effect is modest, with an estimated change in export production of approximately +5.5% leading to low changes in subsurface oxygen concentrations in regions of intense N deposition (< -1% in BoB and about -1% in AS, not shown). These findings contrast with those of Sarma et al. (2022), who estimated a significant contribution of atmospheric sources to export production, particularly in the BoB (17%) compared to the AS (6%), potentially intensifying OMZ formation.

5 Conclusion

This study aims to investigate the potential compensatory role of atmospheric N deposition in mitigating the declining climate-driven trend in marine productivity. To this end, we used a regional ocean biogeochemical model of the northern Indian Ocean to simulate the effect of N deposition and of climate variability on productivity over the contemporary period. The N deposition change increased primary production over the 1980-2020 period (+0.6% for the NIO, +10 mg $C.m^{-2}.d^{-1}.yr^{-1}$ locally) and confirms its fertilizing effect at the basin-scale, consistent with previous estimates. Our results indicate that the total increase in primary production due to N deposition, corresponding to an efficient use of additional nitrogen by phytoplankton (60%), did not induce a significant increase in export efficiency. However, this N deposition effect can locally offset the climate-induced downward trend in primary productivity in the central Arabian Sea and the western Bay of Bengal. One notable limitation of our study is the exclusion of external sources like organic nitrogen and their potential increase such as those from riverine inputs, potentially leading to an underestimation of total reactive nitrogen budget. In

addition to our findings, uncertain projections of NPP evolution in the Indian Ocean from CMIP5 to CMIP6 models reveal a sharp increase in inter-model uncertainties, with a doubling ranging from about -2% to -14% (Tagliabue et al., 2021). Furthermore, many of these projections do not take into account changes in external nitrogen sources, including atmospheric deposition (Séférian et al., 2020), suggesting a need for enhanced understanding and improved modeling approaches. Integrating these insights is crucial for refining our comprehension of the intricate biogeochemical processes governing the northern Indian Ocean, particularly with respect to the role of atmospheric nitrogen deposition.

Data availability statement

The MOM6-IND12 model data presented in the study are deposited in the Zenodo repository: https://zenodo.org/records/14051993. Deposition fields are available at the World Data Center for Climate repository, accession number 10.26050/WDCC/AR6.C6CMNGGFEhi and 10.26050/WDCC/AR6.C6SPNGGFLs585.

Author contributions

MM: Writing – review & editing, Writing – original draft. LR: Writing – review & editing, Writing – original draft. LB: Writing – review & editing, Writing – original draft. YZ: Writing – review & editing, Writing – original draft. SD: Writing – review & editing, Writing – original draft. FY: Writing – review & editing, Writing – original draft. FP: Writing – review & editing, Writing – original draft. ML: Writing – review & editing, Writing – original draft.

Funding

Acknowledgments

Conflict of interest

The authors declare that the research was conducted in the absence of any commercial or financial relationships that could be construed as a potential conflict of interest.

Publisher's note

All claims expressed in this article are solely those of the authors and do not necessarily represent those of their affiliated organizations, or those of the publisher, the editors and the reviewers. Any product that may be evaluated in this article, or claim that may be made by its manufacturer, is not guaranteed or endorsed by the publisher.

Supplementary material

The Supplementary Material for this article can be found online at: https://www.frontiersin.org/articles/10.3389/fmars.2024.1418634/full#supplementary-material

References

Adcroft, A., Anderson, W., Balaji, V., Blanton, C., Bushuk, M., Dufour, C. O., et al. (2019). The gfdl global ocean and sea ice model om4. 0: Model description and simulation features. *J. Adv. Modeling Earth Syst.* 11, 3167–3211. doi: 10.1029/2019MS001726

Altieri, K. E., Fawcett, S. E., and Hastings, M. G. (2021). Reactive nitrogen cycling in the atmosphere and ocean. *Annu. Rev. Earth Planet Sci.* 49, 523–550. doi: 10.1146/annurev-earth-083120-052147

Banerjee, P., and Prasanna Kumar, S. (2014). Dust-induced episodic phytoplankton blooms in the arabian sea during winter monsoon. *J. Geophys. Res.: Oceans* 119, 7123–7138. doi: 10.1002/2014JC010304

Beale, C. A., Paulot, F., Randles, C. A., Wang, R., Guo, X., Clarisse, L., et al. (2022). Large sub-regional differences of ammonia seasonal patterns over India reveal inventory discrepancies. *Environ. Res. Lett.* 17, 104006. doi: 10.1088/1748-9326/ac881f

Bikkina, P., Sarma, V., Kawamura, K., and Bikkina, S. (2021). Dry-deposition of inorganic and organic nitrogen aerosols to the arabian sea: sources, transport and biogeochemical significance in surface waters. *Mar. Chem.* 231, 103938. doi: 10.1016/j.marchem.2021.103938

Boyer, T. P., Garcia, H. E., Locarnini, R. A., Zweng, M. M., Mishonov, A. V., Reagan, J. R., et al. (2018). World ocean atlas. *World Ocean Atlas 2018: Product Documentation*. Ed. A. Mishonov (United States: NOAA Atlas). Technical Ed.

de Boyer Montégut, C., Madec, G., Fischer, A. S., Lazar, A., and Iudicone, D. (2004). Mixed layer depth over the global ocean: An examination of profile data and a profile-based climatology. *J. Geophys. Res.: Oceans* 109. doi: 10.1029/2004JC002378

Duce, R. A., LaRoche, J., Altieri, K., Arrigo, K. R., Baker, A. R., Capone, D. G., et al. (2008). Impacts of atmospheric anthropogenic nitrogen on the open ocean. *Sci.* 320, 893–897. doi: 10.1126/science.1150369

Dunne, J. P., Horowitz, L., Adcroft, A., Ginoux, P., Held, I., John, J., et al. (2020). The gfdl earth system model version 4.1 (gfdl-esm 4.1): Overall coupled model description and simulation characteristics. *J. Adv. Modeling Earth Syst.* 12, e2019MS002015. doi: 10.1029/2019MS002015

Eyring, V., Bony, S., Meehl, G. A., Senior, C. A., Stevens, B., Stouffer, R. J., et al. (2016). Overview of the coupled model intercomparison project phase 6 (cmip6) experimental design and organization. *Geoscientific Model. Dev.* 9, 1937–1958. doi: 10.5194/gmd-9-1937-2016

Gadgil, S. (2003). The Indian monsoon and its variability. *Annu. Rev. Earth Planetary Sci.* 31, 429–467. doi: 10.1146/annurev.earth.31.100901.141251

Guieu, C., Al Azhar, M., Aumont, O., Mahowald, N., Levy, M., Ethé, C., et al. (2019). Major impact of dust deposition on the productivity of the arabian sea. *Geophys. Res. Lett.* 46, 6736–6744. doi: 10.1029/2019GL082770

Hamilton, D. S., Baker, A. R., Iwamoto, Y., Gassó, S., Bergas-Masso, E., Deutch, S., et al. (2023). An aerosol odyssey: Navigating nutrient flux changes to marine ecosystems. *Elem Sci. Anth* 11, 00037. doi: 10.1525/elementa.2023.00037

Hamilton, D. S., Moore, J. K., Arneth, A., Bond, T. C., Carslaw, K. S., Hantson, S., et al. (2020). Impact of changes to the atmospheric soluble iron deposition flux on ocean biogeochemical cycles in the anthropocene. *Global Biogeochemical Cycles* 34, e2019GB006448. doi: 10.1029/2019GB006448

Harrigan, S., Zoster, E., Cloke, H., Salamon, P., and Prudhomme, C. (2020). Daily ensemble river discharge reforecasts and real-time forecasts from the operational global flood awareness system. *Hydrol. Earth Sys. Sci. Discussions* 2020, 1–22. doi: 10.5194/hess-27-1-2023

Herbert, R, Krom, M., Carslaw, K., Stockdale, A., Mortimer, R., Benning, L. G., et al. (2018). The effect of atmospheric acid processing on the global deposition of bioavailable phosphorus from dust. *Global Biogeochemical Cycles* 32, 1367–1385. doi: 10.1029/2018GB005880

Hersbach, H., Bell, B., Berrisford, P., Hirahara, S., Horányi, A., Muñoz-Sabater, J., et al. (2020). The era5 global reanalysis. *Q. J. R. Meteorological Soc.* 146, 1999–2049. doi: 10.1002/qj.v146.730

Hoesly, R. M., Smith, S. J., Feng, L., Klimont, Z., Janssens-Maenhout, G., Pitkanen, T., et al. (2018). Historical, (1750–2014) anthropogenic emissions of reactive gases and aerosols from the community emissions data system (ceds). *Geoscientific Model. Dev.* 11, 369–408. doi: 10.5194/gmd-11-369-2018

Hood, R. R., Coles, V. J., Huggett, J. A., Landry, M. R., Levy, M., Moffett, J. W., et al. (2024). "Nutrient, phytoplankton, and zooplankton variability in the Indian ocean," in *The Indian Ocean and its role in the global climate system.* C. C. Ummenhofer and R. R. Hood Eds. (Elsevier), 293–327. Available online at: https://www.elsevier.com/books-and-journals/book-companion/9780128226988.

Horowitz, L. W., Naik, V., Paulot, F., Ginoux, P. A., Dunne, J. P., Mao, J., et al. (2020). The GFDL global atmospheric chemistry-climate model AM4.1: Model description and simulation characteristics. *J. Adv. Model. Earth Syst.* 12. doi: 10.1029/2019MS002032

Jiang, S., Jin, J., Jiang, S., Wu, Y., Wang, J., Chen, J., et al. (2021). Nitrogen in atmospheric wet depositions over the east Indian ocean and west pacific ocean: Spatial variability, source identification, and potential influences. *Front. Mar. Sci.* 7, 600843. doi: 10.3389/fmars.2020.600843

Jickells, T., An, Z., Andersen, K. K., Baker, A., Bergametti, G., Brooks, N., et al. (2005). Global iron connections between desert dust, ocean biogeochemistry, and climate. *science* 308, 67–71. doi: 10.1126/science.1105959

Jickells, T. D., Buitenhuis, E., Altieri, K., Baker, A. R., Capone, D., Duce, R. A., et al. (2017). A reevaluation of the magnitude and impacts of anthropogenic atmospheric nitrogen inputs on the ocean: Atmospheric nitrogen inputs. *Global Biogeochemical Cycles.* 31 (2), 289–305. doi: 10.1002/2016GB005586

Kalita, R., and Lotliker, A. A. (2023). Assessment of satellite-based net primary productivity models in different biogeochemical provinces over the northern Indian ocean. *Int. J. Remote Sens.*, 1–20. doi: 10.1080/01431161.2023.2247533

Kanakidou, M., Myriokefalitakis, S., Daskalakis, N., Fanourgakis, G., Nenes, A., Baker, A., et al. (2016). Past, present, and future atmospheric nitrogen deposition. *J. Atmospheric Sci.* 73, 2039–2047. doi: 10.1175/JAS-D-15-0278.1

Koné, V., Aumont, O., Lévy, M., and Resplandy, L. (2009). Physical and biogeochemical controls of the phytoplankton seasonal cycle in the Indian ocean: A modeling study. *Indian Ocean Biogeochemical Processes Ecol. Variability* 185, 350. doi: 10.1029/2008GM000700

Kriegler, E., Bauer, N., Popp, A., Humpenöder, F., Leimbach, M., Strefler, J., et al. (2017). Fossil fueled development (ssp5): An energy and resource intensive scenario for the 21st century. *Global Environ. Change* 42, 297–315. doi: 10.1016/j.gloenvcha.2016.05.015

Kumar, S., Ramesh, R., Sardesai, S., and Sheshshayee, M. S. (2004). High new production in the bay of bengal: Possible causes and implications. *Geophys. Res. Lett.* 31, L18304. doi: 10.1029/2004GL021005

Kumari, V., Ghosh, V., Rao, D., Krishna, M., and Sarma, V. (2022a). Nitrogen fixation in the western coastal bay of bengal: Controlling factors and contribution to primary production. *Regional Stud. Mar. Sci.* 53, 102410. doi: 10.1016/j.rsma.2022.102410

Kumari, V., Sarma, V., and Kumar, M. D. (2022b). Spatial variability in aerosol composition and its seawater acidification potential in coastal waters of the western coastal bay of bengal. *J. Earth Sys. Sci.* 131, 251. doi: 10.1007/s12040-022-01996-w

Kumari, V., Yadav, K., Sarma, V., and Dileep Kumar, M. (2021). Acidification of the coastal bay of Bengal by aerosols deposition. *J. Earth Sys. Sci.* 130, 1–13. doi: 10.1007/s12040-021-01723-x

Lachkar, Z., Mehari, M., Al Azhar, M., Lévy, M., and Smith, S. (2021). Fast local warming is the main driver of recent deoxygenation in the northern arabian sea. *Biogeosci.* 18, 5831–5849. doi: 10.5194/bg-18-5831-2021

Lévy, M., Shankar, D., André, J.-M., Shenoi, S., Durand, F., and de Boyer Montégut, C. (2007). Basin wide seasonal evolution of the Indian ocean's phytoplankton blooms. *J. Geophys. Res.: Oceans* 112. doi: 10.1029/2007JC004090

Locarnini, M., Mishonov, A., Baranova, O., Boyer, T., Zweng, M., Garcia, H., et al. (2018). National Oceanic and Atmospheric Administration National Environmental Satellite, Data, and Information Service National Centers for Environmental Information. *World ocean atlas 2018, volume 1: Temperature.* NOAA Atlas NESDIS 81, 52pp.

Maishal, S. (2024). Unraveling the declining Indian ocean primary productivity and key drivers. *Discover Oceans* 1, 17. doi: 10.1007/s44289-024-00018-5

Mayorga, E., Seitzinger, S. P., Harrison, J. A., Dumont, E., Beusen, A. H., Bouwman, A., et al. (2010). enGlobal Nutrient Export from WaterSheds 2 (NEWS 2): Model development and implementation. *Environ. Model. Softw.* 25, 837–853. doi: 10.1016/j.envsoft.2010.01.007

McDuffie, E. E., Smith, S. J., O'Rourke, P., Tibrewal, K., Venkataraman, C., Marais, E. A., et al. (2020). A global anthropogenic emission inventory of atmospheric pollutants from sector-and fuel-specific sources, (1970–2017): an application of the community emissions data system (ceds). *Earth Sys. Sci. Data* 12, 3413–3442. doi: 10.5194/essd-12-3413-2020

Morrison, J. M., Codispoti, L., Gaurin, S., Jones, B., Manghnani, V., and Zheng, Z. (1998). Seasonal variation of hydrographic and nutrient fields during the us jgofs arabian sea process study. *Deep Sea Res. Part II: Topical Stud. Oceanogr.* 45, 2053–2101. doi: 10.1016/S0967-0645(98)00063-0

O'Neill, B. C., Tebaldi, C., Van Vuuren, D. P., Eyring, V., Friedlingstein, P., Hurtt, G., et al. (2016). The scenario model intercomparison project (scenariomip) for cmip6. *Geoscientific Model. Dev.* 9, 3461–3482. doi: 10.5194/gmd-9-3461-2016

Olsen, A., Key, R. M., Van Heuven, S., Lauvset, S. K., Velo, A., Lin, X., et al. (2016). The global ocean data analysis project version 2 (glodapv2)–an internally consistent data product for the world ocean. *Earth Sys. Sci. Data* 8, 297–323. doi: 10.5194/essd-8-297-2016

Patra, P. K., Kumar, M. D., Mahowald, N., and Sarma, V. (2007a). Atmospheric deposition and surface stratification as controls of contrasting chlorophyll abundance in the north Indian ocean. *J. Geophys. Res.: Oceans* 112. doi: 10.1029/2006JC003885

Patra, P. K., Kumar, M. D., Mahowald, N., and Sarma, V. V. S. S. (2007b). Atmospheric deposition and surface stratification as controls of contrasting chlorophyll abundance in the north Indian ocean 112. doi: 10.1029/2006JC003885

Paulot, F., Stock, C., John, J. G., Zadeh, N., and Horowitz, L. W. (2020). Ocean ammonia outgassing: Modulation by CO2 and anthropogenic nitrogen deposition. *J. Adv. Model Earth Syst.* 12. doi: 10.1029/2019MS002026

Pedde, S., Kroeze, C., Mayorga, E., and Seitzinger, S. P. (2017). Modeling sources of nutrients in rivers draining into the bay of bengal—a scenario analysis. *Regional Environ. Change* 17, 2495–2506. doi: 10.1007/s10113-017-1176-7

Peng, S., and Wang, Q. (2024). Fast enhancement of the stratification in the Indian ocean over the past 20 years. *J. Climate.* 37 (7), 2231–2245. doi: 10.1175/JCLI-D-23-0255.1

Prakash, S., and Ramesh, R. (2007). *Is the arabian sea getting more productive?* Vol. 92 (New- York City USA: Temporary Publisher), 667–671.

Raiswell, R., and Canfield, D. E. (2012). The iron biogeochemical cycle past and present. *Geochemical Perspect.* 1, 1–220. doi: 10.7185/geochempersp.1.1

Resplandy, L., Lévy, M., Madec, G., Pous, S., Aumont, O., and Kumar, D. (2011). Contribution of mesoscale processes to nutrient budgets in the arabian sea. *J. Geophys. Res.: Oceans* 116. doi: 10.1029/2011JC007006

Ross, A. C., Stock, C. A., Adcroft, A., Curchitser, E., Hallberg, R., Harrison, M. J., et al. (2023). A high-resolution physical-biogeochemical model for marine resource applications in the northwest atlantic (mom6-cobalt-nwa12 v1. 0). *Geoscientific Model. Dev. Discussions* 2023, 1–65. doi: 10.5194/gmd-16-6943-2023

Roxy, M. K., Modi, A., Murtugudde, R., Valsala, V., Panickal, S, Prasanna Kumar, S., et al. (2016). A reduction in marine primary productivity driven by rapid warming over the tropical Indian ocean. *Geophys. Res. Lett.* 43, 826–833. doi: 10.1002/2015GL066979

Sarma, V., Krishna, M., Paul, Y., and Murty, V. (2015). Observed changes in ocean acidity and carbon dioxide exchange in the coastal bay of bengal–a link to air pollution. *Tellus B: Chem. Phys. Meteorol.* 67, 24638. doi: 10.3402/tellusb.v67.24638

Sarma, V., Rao, D., Rajula, G., Dalabehera, H., and Yadav, K. (2019). Organic nutrients support high primary production in the bay of bengal. *Geophys. Res. Lett.* 46, 6706–6715. doi: 10.1029/2019GL082262

Sarma, V. V. S. S., Sridevi, B., Kumar, A., Bikkina, S., Kumari, V. R., Bikkina, P., et al. (2022). *Impact of atmospheric anthropogenic nitrogen on new production in the northern Indian ocean: constrained based on satellite aerosol optical depth and particulate nitrogen levels* Vol. 24 (Cambridge UK: The Royal Society of Chemistry), 1895–1911. doi: 10.1039/D2EM00234E

Sarma, V., Vivek, R., Rao, D., and Ghosh, V. (2020). Severe phosphate limitation on nitrogen fixation in the bay of bengal. *Continental Shelf Res.* 205, 104199. doi: 10.1016/j.csr.2020.104199

Sathyendranath, S., Brewin, R. J., Brockmann, C., Brotas, V., Calton, B., Chuprin, A., et al. (2019). An ocean-colour time series for use in climate studies: the experience of the ocean-colour climate change initiative (oc-cci). *Sensors* 19, 4285. doi: 10.3390/s19194285

Schott, F. A., and McCreary, J. P. Jr. (2001). The monsoon circulation of the Indian ocean. *Prog. Oceanogr.* 51, 1–123. doi: 10.1016/S0079-6611(01)00083-0

Séférian, R., Berthet, S., Yool, A., Palmiéri, J., Bopp, L., Tagliabue, A., et al. (2020). Tracking improvement in simulated marine biogeochemistry between cmip5 and cmip6. *Curr. Climate Change Rep.* 6, 95–119. doi: 10.1007/s40641-020-00160-0

Shankar, D., Vinayachandran, P., and Unnikrishnan, A. (2002). The monsoon currents in the north Indian ocean. *Prog. Oceanogr.* 52, 63–120. doi: 10.1016/S0079-6611(02)00024-1

Sharma, S., Ha, K.-J., Yamaguchi, R., Rodgers, K. B., Timmermann, A., and Chung, E.-S. (2023). Future Indian ocean warming patterns. *Nat. Commun.* 14, 1789. doi: 10.1038/s41467-023-37435-7

Singh, A., Gandhi, N., and Ramesh, R. (2012). Contribution of atmospheric nitrogen deposition to new production in the nitrogen limited photic zone of the northern Indian ocean 117. doi: 10.1029/2011JC007737

Singh, A., and Ramesh, R. (2011). *Contribution of riverine dissolved inorganic nitrogen flux to new production in the coastal northern Indian ocean: An assessment* Vol. 2011 (Hindawi). doi: 10.1155/2011/983561

Sinha, N., Chakraborty, S., Chattopadhyay, R., Goswami, B., Mohan, P., Parua, D. K., et al. (2019). Isotopic investigation of the moisture transport processes over the bay of bengal. *J. Hydrol. X* 2, 100021. doi: 10.1016/j.hydroa.2019.100021

Sipler, R. E., and Bronk, D. A. (2015). "Dynamics of dissolved organic nitrogen," in *Biogeochemistry of marine dissolved organic matter* (Amsterdam, The Netherlands: Elsevier), 127–232.

Sridevi, B., Sabira, S., and Sarma, V. (2023). Impact of ocean warming on net primary production in the northern Indian ocean: role of aerosols and freshening of surface ocean. *Environ. Sci. pollut. Res.* 30, 53616–53634. doi: 10.1007/s11356-023-26001-9

Sridevi, B., and Sarma, V. V. S. S. (2022). Enhanced atmospheric pollutants strengthened winter convective mixing and phytoplankton blooms in the northern arabian sea. *J. Geophys. Res. Biogeosci.* 127. doi: 10.1029/2021JG006527

Srinivas, B., and Sarin, M. M. (2013). Atmospheric deposition of n, p and fe to the northern Indian ocean: Implications to c- and n-fixation. *Science of The Total Environment* 456-457, 104–114. doi: 10.1016/j.scitotenv.2013.03.068

Srinivas, B., Sarin, M. M., and Sarma, V. V. S. S. (2011). Atmospheric dry deposition of inorganic and organic nitrogen to the bay of bengal: Impact of continental outflow. *Marine Chemistry* 127, 170–179. doi: 10.1016/j.marchem.2011.09.002

Stock, C. A., Dunne, J. P., Fan, S., Ginoux, P., John, J., Krasting, J. P., et al. (2020). Ocean biogeochemistry in GFDL's earth system model 4.1 and its response to increasing atmospheric CO. *J. Adv. Model Earth Syst.* 2, 12. doi: 10.1029/2019MS002043

Stock, C. A., Dunne, J. P., and John, J. G. (2014). Global-scale carbon and energy flows through the marine planktonic food web: An analysis with a coupled physical–biological model. *Prog. Oceanogr.* 120, 1–28. doi: 10.1016/j.pocean.2013.07.001

Suntharalingam, P., Zamora, L. M., Bange, H. W., Bikkina, S., Buitenhuis, E., Kanakidou, M., et al. (2019). Anthropogenic nitrogen inputs and impacts on oceanic n2o fluxes in the northern Indian ocean: The need for an integrated observation and modelling approach. *Deep Sea Research Part II: Topical Studies in Oceanography* 166, 104–113. doi: 10.1016/j.dsr2.2019.03.007

Tagliabue, A., Kwiatkowski, L., Bopp, L., Butenschön, M., Cheung, W., Lengaigne, M., et al. (2021). Persistent uncertainties in ocean net primary production climate change projections at regional scales raise challenges for assessing impacts on ecosystem services. *Front. Climate* 3. doi: 10.3389/fclim.2021.738224

Thangaradjou, T., Sarangi, R., Shanthi, R., Poornima, D., Raja, K., Saravanakumar, A., et al. (2014). Changes in nutrients ratio along the central bay of bengal coast and its influence on chlorophyll distribution. *J. Environ. Biol.* 35, 467.

Twining, B. S., Rauschenberg, S., Baer, S. E., Lomas, M. W., Martiny, A. C., and Antipova, O. (2019). A nutrient limitation mosaic in the eastern tropical Indian ocean. *Deep Sea Res. Part II: Topical Stud. Oceanogr.* 166, 125–140. doi: 10.1016/j.dsr2.2019.05.001

Westberry, T., Behrenfeld, M., Siegel, D., and Boss, E. (2008). Carbon-based primary productivity modeling with vertically resolved photoacclimation. *Global Biogeochemical Cycles* 22. doi: 10.1029/2007GB003078

Wiggert, J. D., Hood, R., Banse, K., and Kindle, J. (2005). Monsoon-driven biogeochemical processes in the arabian sea. *Prog. Oceanogr.* 65, 176–213. doi: 10.1016/j.pocean.2005.03.008

Wiggert, J., Murtugudde, R., and Christian, J. (2006a). Annual ecosystem variability in the tropical Indian ocean: Results of a coupled bio-physical ocean general circulation model. *Deep Sea Research Part II: Topical Studies in Oceanography* 53, 644–676. doi: 10.1016/j.dsr2.2006.01.027

Wiggert, J., Murtugudde, R., and Christian, J. (2006b). Annual ecosystem variability in the tropical Indian ocean: Results of a coupled bio-physical ocean general circulation model. *Deep Sea Res. Part II: Topical Stud. Oceanogr.* 53, 644–676. doi: 10.1016/j.dsr2.2006.01.027

Yadav, K., Rao, V., Sridevi, B., and Sarma, V. (2021). Decadal variations in natural and anthropogenic aerosol optical depth over the bay of bengal: the influence of pollutants from indo-gangeticplain. *Environ. Sci. pollut. Res.* 28, 55202–55219. doi: 10.1007/s11356-021-14703-x

Yadav, K., Sarma, V., Rao, D., and Kumar, M. D. (2016). Influence of atmospheric dry deposition of inorganic nutrients on phytoplankton biomass in the coastal bay of bengal. *Mar. Chem.* 187, 25–34. doi: 10.1016/j.marchem.2016.10.004

Yuan, Z., Achterberg, E. P., Engel, A., Wen, Z., Zhou, L., Zhu, X., et al. (2023). Phytoplankton community response to episodic wet and dry aerosol deposition in the subtropical north atlantic. *Limnol. Oceanogr.* 68, 2126–2140. doi: 10.1002/lno.12410

Zuo, H., Balmaseda, M. A., Tietsche, S., Mogensen, K., and Mayer, M. (2019). The ecmwf operational ensemble reanalysis–analysis system for ocean and sea ice: a description of the system and assessment. *Ocean Sci.* 15, 779–808. doi: 10.5194/os-15-779-2019

Zweng, M., Seidov, D., Boyer, T., Locarnini, M., Garcia, H., Mishonov, A., et al. (2019). *World ocean atlas 2018, volume 2: Salinity*. (National Oceanic and Atmospheric Administration National Environmental Satellite, Data, and Information Service National Centers for Environmental Information NOAA/NESDIS National Centers for Environmental Information SSMC3, 4th floor 1315 East-West Highway Silver Spring, MD 20910-3282).